INTERNATIONAL JOURNAL FOR NUMERICAL METHODS IN FLUIDS
Int. J. Numer. Meth. Fluids 2002; **38**:125–138 (DOI: 10.1002/fld.205)

An implicit velocity decoupling procedure for the incompressible Navier–Stokes equations

Kyoungyoun Kim, Seung-Jin Baek and Hyung Jin Sung*,†

Department of Mechanical Engineering, Korea Advanced Institute of Science and Technology, 373-1, Kusong-dong, Yusong-ku, Taejon, 305-701, Korea

SUMMARY

An efficient numerical method to solve the unsteady incompressible Navier–Stokes equations is developed. A fully implicit time advancement is employed to avoid the Courant–Friedrichs–Lewy restriction, where the Crank–Nicolson discretization is used for both the diffusion and convection terms. Based on a block LU decomposition, velocity–pressure decoupling is achieved in conjunction with the approximate factorization. The main emphasis is placed on the additional decoupling of the intermediate velocity components with only *n*th time step velocity. The temporal second-order accuracy is preserved with the approximate factorization without any modification of boundary conditions. Since the decoupled momentum equations are solved without iteration, the computational time is reduced significantly. The present decoupling method is validated by solving several test cases, in particular, the turbulent minimal channel flow unit. Copyright © 2002 John Wiley & Sons, Ltd.

KEY WORDS: incompressible Navier–Stokes equations; implicit time advancement; velocity–pressure decoupling; velocity componets decoupling; second-order accuracy; approximate factorization

1. INTRODUCTION

Recent advances in direct numerical simulation (DNS) and large eddy simulation (LES) have intensified the interest to develop more efficient numerical algorithms in solving the incompressible Navier–Stokes equations. Central to the success, among others, is the decoupling of the coupled set of incompressible momentum and continuity equations, although new splitting errors are introduced. Based on the splitting method of Chorin [1], Kim and Moin [2] proposed a fractional-step method in which velocity and pressure are split while preserving the temporal second-order accuracy. The intermediate velocity field is computed by ignoring the incompressibility constraint at the first step and then projected onto a divergence-free field in the second step to obtain the velocity field at the new time level.

*Correspondence to: H. J. Sung, Dept. of Mechanical Engineering, Korea Advanced Institute of Science and Technology, 373-1, Kusong-dong, Yusong-ku, Taejon, 305-701, Korea.
† E-mail: hjsung@kaist.ac.kr

Received September 2000
Revised April 2001

A literature survey reveals that many versions of the fractional step method have been documented [3–6]. Despite the apparent advantages and extensive use in the past by numerous researchers, it is known that the splitting method has several major drawbacks, i.e. low accuracy in time integration and subtle boundary conditions for the intermediate velocity and pressure. The preservation of second-order temporal accuracy of the method is not straightforward, and the inherent splitting errors might degrade the solution to a first-order [7, 8]. The poor temporal accuracy is not due to the boundary conditions, but due to the method itself. Recently, Perot [7] and Dukowicz and Dvinsky [9] proposed the full discretized equations, in which the governing equations were written in matrix form by being discretized temporally and spatially at once. The boundary conditions have been already incorporated and, therefore, no *ad-hoc* boundary conditions of the intermediate variables were required to preserve the temporal second-order accuracy exactly. They also analyzed the full discretized equations with an approximate factorization method [9] and a block LU decomposition method [7], respectively.

A perusal of the relevant studies indicates that most of the afore-stated methods have used a semi-implicit scheme where the implicit scheme is used for the viscous terms and the explicit scheme is used for the nonlinear convective terms. Accordingly, the advancement of computational time step is restricted owing to the limitation of the Courant–Friedrichs–Lewy (CFL) number. Additional computational time steps are required to maintain the numerical stability. A fully implicit method where all terms in the momentum equations are advanced with the Crank–Nicholson method in time is preferred when the time step limit imposed by an explicit or semi-implicit stability bound must be significantly less than the time step requirements, i.e. the smallest physical flow time scale. Choi and Moin [10] adopted a fully implicit method based on the fractional step method, in which the spatial discretization is made after the temporal splitting of the Navier–Stokes equations. However, the intermediate velocity components are coupled due to the implicit treatment of the convective terms. A Newton-iterative method has been employed to solve the first step from which the coupled intermediate velocity components are obtained [10, 11]. To avoid this iterative procedure, Rosenfeld [12] proposed an uncoupled implicit solver in which all of the governing equations are uncoupled without degrading temporal accuracy or stability. He devised the three-time-level linearization scheme, however, this scheme requires the velocity field at the time level $n-1$ as well as n to obtain the velocity at the time level $n+1$.

In the present study, a new fully implicit decoupling method is proposed. Based on a block LU decomposition, velocity and pressure are decoupled preserving the temporal second-order accuracy in conjunction with the method of approximate factorization. Furthermore, since the intermediate velocity components are coupled due to the implicit Crank–Nicholson representation for the convective terms, additional decoupling for the intermediate velocity components is achieved by the approximate factorization with only nth time step velocity. These decoupling procedures also preserve the second-order accuracy in time. The present decoupling method is described in detail in Section 2. In Section 3, the temporal second-order accuracy for the present method is ascertained by computing the flow with initial vortex. The stability of velocity components decoupling procedure is tested. The impulsively started lid-driven cavity flow is calculated to validate the present decoupling method. The present decoupling method is applied to the minimal channel flow unit with DNS. A summary is given in Section 4.

2. NUMERICAL METHODS

The nondimensional governing equations for an unsteady incompressible flow are

$$\frac{\partial u_i}{\partial t} + \frac{\partial}{\partial x_j} u_i u_j = -\frac{\partial p}{\partial x_i} + \frac{1}{Re} \frac{\partial}{\partial x_j} \frac{\partial u_i}{\partial x_j}, \quad (i = 1, 2, 3) \tag{1}$$

$$\frac{\partial u_i}{\partial x_i} = 0 \tag{2}$$

where x_i are the Cartesian coordinates and u_i are the corresponding velocity components in each direction. All variables are non-dimensionalized by a characteristic length and velocity scale, and Re is the Reynolds number.

At the $n + 1/2$ time level, straightforward spatial and temporal discretization of Equations (1) and (2) can be accomplished in the form,

$$\frac{\boldsymbol{u}^{n+1} - \boldsymbol{u}^n}{\Delta t} + \frac{1}{2}(H(\boldsymbol{u}^{n+1}) + H(\boldsymbol{u}^n)) = -Gp^{n+1/2} + \frac{1}{2Re}(L\boldsymbol{u}^{n+1} + L\boldsymbol{u}^n) + \boldsymbol{mbc} \tag{3}$$

$$D\boldsymbol{u}^{n+1} = 0 + cbc \tag{4}$$

where L represents the discrete Laplacian viscous operator, H is the discrete convective operator, G is the discrete gradient operator and D is the discrete divergence operator, respectively. Here, Δt is the time increment and the superscript n denotes the nth time step.

It is important to note that the boundary conditions have already been incorporated in Equations (3) and (4). The spatial discrete operators L, H, G and D are evaluated using a second-order central finite-difference scheme on a staggered grid. The unknown variables $\boldsymbol{u}^{n+1}$ and $p^{n+1/2}$ refer to the nodes in the interior, not to the boundary nodes in the staggered grid system. The known velocities at the boundary, i.e. boundary conditions for the velocities, have been imposed on $\boldsymbol{mbc}$ and cbc, respectively [7, 8]. On the staggered grid, pressure is defined at the cubic cell center while each unknown velocity component is defined at the center of orthogonal plane to each velocity component. Accordingly, discretization of the momentum equations at the boundary requires neither the pressure gradient nor the pressure itself at the boundary.

For temporal discretization, we have used a fully implicit time-advancement where all terms in Equation (1) are advanced with the second-order Crank–Nicholson scheme in time. It is known that the Crank–Nicholson scheme is not strongly A-stable. However, the Crank–Nicholson scheme preserves free oscillations well [6]. An implicit treatment of both the convective and the viscous terms yields nonlinear equations since the velocities of the nonlinear convective terms are unknown. In the present study, the nonlinear terms are linearized by employing the procedure of Beam and Warming [13] with second-order temporal accuracy.

$$u_i^{n+1} u_j^{n+1} = u_i^{n+1} u_j^n + u_i^n u_j^{n+1} - u_i^n u_j^n + O(\Delta t^2) \tag{5}$$

By this linearization, a linear operator for the convective term N can be defined as,

$$N\boldsymbol{u}^{n+1} = \frac{1}{2}(H(\boldsymbol{u}^{n+1}) + H(\boldsymbol{u}^{n})) \tag{6}$$

Note that the convective operator N includes only the velocity at the time level n.

The discretized Equations (3) and (4) can be rewritten in matrix form by using the above convective operator N.

$$\begin{pmatrix} A & G \\ D & 0 \end{pmatrix} \begin{pmatrix} \boldsymbol{u}^{n+1} \\ \delta p \end{pmatrix} = \begin{pmatrix} \boldsymbol{r} \\ 0 \end{pmatrix} + \begin{pmatrix} \boldsymbol{mbc} \\ cbc \end{pmatrix} \tag{7}$$

$$A = \frac{1}{\Delta t}\left[I + \Delta t\left(N - \frac{1}{2Re}L\right)\right]$$

$$\boldsymbol{r} = \frac{1}{\Delta t}\boldsymbol{u}^{n} - Gp^{n-1/2} + \frac{1}{2Re}L\mathbf{u}^{n}$$

$$\delta p = p^{n+1/2} - p^{n-1/2}$$

In the above, $\boldsymbol{u}^{n+1}$ and $p^{n+1/2}$ at the next time step can be obtained by making an inversion of the coefficient matrix of Equation (7). However, since the coefficient matrix is very large and sparse, it is difficult and time-consuming to solve Equation (7) directly. In other words, Equation (7) may not be solved explicitly since velocity and pressure are linked implicitly in the momentum equation and continuity equation.

Equation (7) can be factored into the block LU decomposition as

$$\begin{pmatrix} A & 0 \\ D & -\Delta tDG \end{pmatrix} \begin{pmatrix} I & \Delta tG \\ 0 & I \end{pmatrix} \begin{pmatrix} \boldsymbol{u}^{n+1} \\ \delta p \end{pmatrix} = \begin{pmatrix} \boldsymbol{r} \\ 0 \end{pmatrix} + \begin{pmatrix} \boldsymbol{mbc} \\ cbc \end{pmatrix} \tag{8}$$

Note that this differs from Equation (7) by an approximation of $G\delta p$ to $\Delta tAG\delta p$, which arises as a consequence of the approximate factorization. The pressure in the present study is expressed by the so-called 'delta form δp' [14]. This is to make the above approximate factorization second-order in time, i.e. the error term is $O(\Delta t^2)$ as

$$O(\Delta t^2) = \begin{pmatrix} \Delta tMG\delta p \\ 0 \end{pmatrix}, \quad \text{where } M = N - \frac{1}{2Re}L \tag{9}$$

Equation (8) can be rewritten as

$$\begin{pmatrix} A & 0 \\ D & -\Delta tDG \end{pmatrix} \begin{pmatrix} \boldsymbol{u}^{*} \\ \delta p \end{pmatrix} = \begin{pmatrix} \boldsymbol{r} \\ 0 \end{pmatrix} + \begin{pmatrix} \boldsymbol{mbc} \\ cbc \end{pmatrix} \tag{10}$$

$$\begin{pmatrix} I & \Delta tG \\ 0 & I \end{pmatrix} \begin{pmatrix} \boldsymbol{u}^{n+1} \\ \delta p \end{pmatrix} = \begin{pmatrix} \boldsymbol{u}^{*} \\ \delta p \end{pmatrix} \tag{11}$$

where $\boldsymbol{u}^*$ is the intermediate value of $\boldsymbol{u}^{n+1}$. A further simplification of these results in the series of operations:

$$A\boldsymbol{u}^* = \boldsymbol{r} + \boldsymbol{mbc} \tag{12}$$

$$\Delta tDG\delta p = D\boldsymbol{u}^* - cbc \tag{13}$$

$$\boldsymbol{u}^{n+1} = \boldsymbol{u}^* - \Delta tG\delta p \tag{14}$$

$$p^{n+1/2} = p^{n-1/2} + \delta p \tag{15}$$

No specific treatment of boundary conditions is required for the intermediate velocities as the boundary conditions have already been applied at the level of Equations (3) and (4). It is found that the velocity–pressure decoupling is achieved without the loss of accuracy in time through Equations (12)–(15).

Next, the afore-stated approximate factorization is further extended to the velocity components $\boldsymbol{u}^*$ in Equation (12) by using the 'delta form $\delta\boldsymbol{u}^*$'. Equation (12) is rewritten with the delta formulation $\delta\boldsymbol{u}^*$ as,

$$A\delta\boldsymbol{u}^* = -A\boldsymbol{u}^n + \boldsymbol{r} + \boldsymbol{mbc} \equiv \boldsymbol{R} \tag{16}$$

$$\delta\boldsymbol{u}^* = \boldsymbol{u}^* - \boldsymbol{u}^n \tag{17}$$

Equation (16) can be expressed in matrix form,

$$\frac{1}{\Delta t}\begin{pmatrix} I + \Delta tM_{11} & \Delta tM_{12} & \Delta tM_{13} \\ \Delta tM_{21} & I + \Delta tM_{22} & \Delta tM_{23} \\ \Delta tM_{31} & \Delta tM_{32} & I + \Delta tM_{33} \end{pmatrix} \begin{pmatrix} \delta u_1^* \\ \delta u_2^* \\ \delta u_3^* \end{pmatrix} = \begin{pmatrix} R_1 \\ R_2 \\ R_3 \end{pmatrix} \tag{18}$$

In Equation (18), the off-diagonal submatrix $M_{ij}(i \neq j)$ is zero when the momentum equations are discretized by semi-implicit methods. However, in the present fully implicit representation, $M_{ij}(i \neq j)$ is no longer zero due to the implicit treatment of the nonlinear convection terms. This implies that δu_1^*, δu_2^* and δu_3^* are fully coupled. By using the approximate factorization of the coefficient matrix in Equation (18), these intermediate velocity components can be decoupled with the only nth time step velocity. Note that the second-order temporal accuracy is also preserved with the approximate factorization.

$$\frac{1}{\Delta t}\begin{pmatrix} I + \Delta tM_{11} & 0 & 0 \\ \Delta tM_{21} & I + \Delta tM_{22} & 0 \\ \Delta tM_{31} & \Delta tM_{32} & I + \Delta tM_{33} \end{pmatrix} \begin{pmatrix} I & \Delta tM_{12} & \Delta tM_{13} \\ 0 & I & \Delta tM_{23} \\ 0 & 0 & I \end{pmatrix} \begin{pmatrix} \delta u_1^* \\ \delta u_2^* \\ \delta u_3^* \end{pmatrix} = \begin{pmatrix} R_1 \\ R_2 \\ R_3 \end{pmatrix} \tag{19}$$

As mentioned earlier, the present decoupling procedure requires only the velocity at t_n. In the prior three-time-level scheme [12, 13] however, the velocities at both t_{n-1} and t_n were employed to preserve the second-order accuracy in time. The second-order error term of Equation (19) is

$$O(\Delta t^2)=\begin{pmatrix} \Delta tM_{11}M_{12}\delta u_2^* + \Delta tM_{11}M_{13}\delta u_3^* \\ \Delta tM_{21}M_{12}\delta u_2^* + \Delta tM_{21}M_{13}\delta u_3^* + \Delta tM_{22}M_{23}\delta u_3^* \\ \Delta tM_{31}M_{12}\delta u_2^* + \Delta tM_{31}M_{13}\delta u_3^* + \Delta tM_{32}M_{23}\delta u_3^* \end{pmatrix} \tag{20}$$

Here, the intermediate terms $\delta \boldsymbol{u}^*$ can be calculated separately in the following steps, which are exactly equivalent to Equation (19) with new variables δu_1^{**} and δu_2^{**}.

$$\frac{1}{\Delta t}(I+\Delta tM_{11})\,\delta u_1^{**}=R_1 \tag{21}$$

$$\frac{1}{\Delta t}(I+\Delta tM_{22})\delta u_2^{**}=R_2-M_{21}\delta u_1^{**} \tag{22}$$

$$\frac{1}{\Delta t}(I+\Delta tM_{33})\delta u_3^{*}=R_3-M_{31}\delta u_1^{**}-M_{32}\delta u_2^{**} \tag{23}$$

$$\delta u_2^{*}=\delta u_2^{**}-\Delta tM_{23}\delta u_3^{*} \tag{24}$$

$$\delta u_1^{*}=\delta u_1^{**}-\Delta tM_{12}\delta u_2^{*}-\Delta tM_{13}\delta u_3^{*} \tag{25}$$

$$u_i^{*}=u_i^{n}+\delta u_i^{*}, \quad (i=1,2,3) \tag{26}$$

As seen in the above equations, the intermediate velocity δu_i^* is obtained by the inversion of only three sub-matrices $[(1)/(\Delta t)](I+\Delta tM_{ii})$ (no summation on i, $i=1,2,3$) with updating the results, instead of the inversion of a large matrix in Equation (12).

M_{ii} is split into three parts such that M_{ii}^1, M_{ii}^2 and M_{ii}^3 contain the derivatives of x_1, x_2 and x_3, respectively. Equation (21) can be rewritten as,

$$\frac{1}{\Delta t}\{I+\Delta t(M_{11}^1+M_{11}^2+M_{11}^3)\}\delta u_1^{**}=R_1 \tag{27}$$

The left-hand side of Equation (27) is then approximated with preserving the temporal second-order accuracy [15],

$$\frac{1}{\Delta t}(I+\Delta tM_{11}^1)(I+\Delta tM_{11}^2)(I+\Delta tM_{11}^3)\delta u_1^{**}=R_1 \tag{28}$$

Equation (28) requires inversions of tridiagonal matrices rather than inversion of a large sparse matrix, as in Equation (27). The same approximate factorization has been applied to Equations (22) and (23). This results in a significant reduction in computing cost and memory by avoiding the inversion of a large sparse matrix of Equations (21)–(23).

The overall numerical computation procedure is as follows:

1. Solve $\boldsymbol{u}^*$ from Equations (21)–(26) through the velocity decoupling procedure.
2. Solve δp from Equation (13).
3. Obtain $\boldsymbol{u}^{n+1}$ from Equation (14), which is a divergence-free vector field, and then one time step marching is finished.

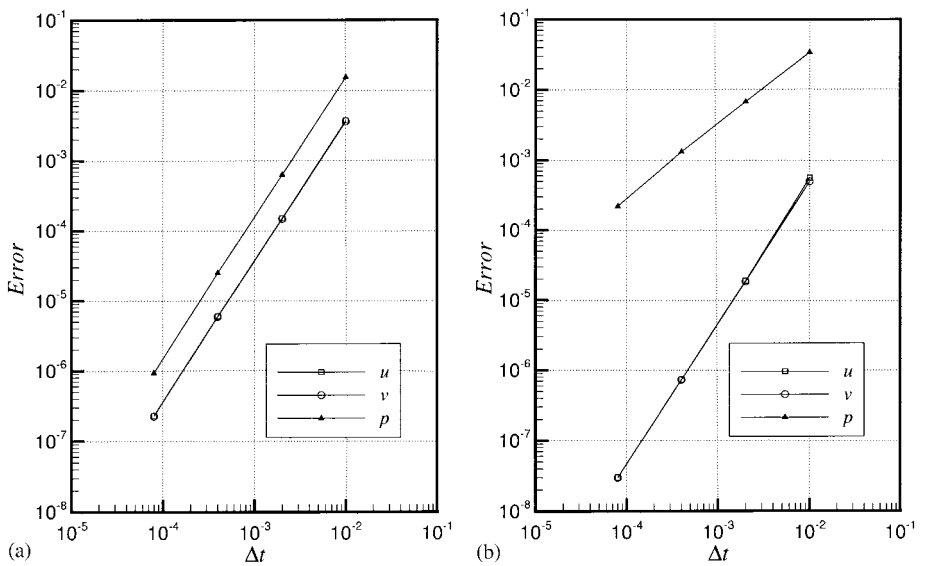

Figure 1. Temporal convergence of the velocity and pressure errors. (a) The present method ($Gp^{n+1/2}$); (b) the trapezoidal pressure update method ($\frac{1}{2}(Gp^{n+1} + Gp^n)$).

3. RESULTS AND DISCUSSION

First of all, it is important to ascertain the second-order accuracy preservation of the present decoupling method. Toward this end, a numerical simulation of the unsteady Navier–Stokes equations in a square domain of unit length ($0 \leqslant x \leqslant 1, 0 \leqslant y \leqslant 1$) is performed. This is the same test case ($Re = 5,000$) as of Perot [7]. The initial condition is a vortex flow given by

$$u^0 = (1 - \cos(2\pi x)) \sin(2\pi y) \tag{29}$$

$$v^0 = (\cos(2\pi y) - 1) \sin(2\pi x) \tag{30}$$

Periodic boundary conditions are imposed at the domain boundaries. To check the temporal accuracy, computations are carried out with various computational time steps on a uniform mesh of 64×64 grids. The solution obtained using the smallest Δt is interpreted as the 'correct solution'. The error in the solutions obtained at increasing Δt is formed by calculating the root-mean-square of the difference in the solution for a given Δt when compared with the 'correct solution'. Measurements of velocities are made at a time ($t = 0.1$) that corresponds to the 10 time steps with the largest computational time step. For the evaluation of 'pressure' error, measurements are made at a time ($t = 0.095$), which corresponds to the $9 + 1/2$ step for the largest time step. Note that the pressure unknown ($p^{n+1/2}$) represents the pressure at the time level $n + 1/2$ whereas the velocity unknowns (u^{n+1}) represent the velocities at the time level $n + 1$. Figure 1(a) shows the errors as a function of the computational time step. As seen, the slope of the curvature is two, which guarantees the second-order accuracy in time for velocity and pressure.

Table I. Errors at different Δt.

Δt	Decoupling scheme	Iterative scheme
0.8E-4	0.2282E-6	0.2276E-6
0.4E-3	0.6094E-5	0.5993E-5
0.2E-2	0.1511E-3	0.1504E-3
0.1E-1	0.3742E-2	0.3695E-2

When the pressure scheme is represented by $\alpha Gp^{n+1} + (1-\alpha)Gp^n$, instead of the present representation $Gp^{n+1/2}$, it is found that the discrete pressure is always first-order accurate in time [7, 8]. Here, α is a scalar varying from 0 to 1. In the present study, the order of accuracy of the pressure update is validated by employing the above scheme with $\alpha = \frac{1}{2}$. An inspection of the temporal convergence of errors in Figure 1(b) indicates that the pressure error deteriorates to the first-order accuracy while the velocity errors keep the second-order accuracy. This suggests that the adoption of $Gp^{n+1/2}$ in Equation (3) is essential to preserve the second-order accuracy for pressure.

Next, to evaluate the attainable time steps to reach a certain accuracy, a comparison is made between the present decoupling method and the conventional iterative method (Equation (18)). As listed in Table I, the error difference for u is negligible. This suggests that the present method is efficient in saving the computational time and memory.

Before proceeding further, a discrete perturbation analysis is carried out to check the stability of the decoupling of velocity components in the convective terms. The following two-dimensional nonlinear hyperbolic equations are adopted, where the velocity components are coupled in the convective terms:

$$\frac{\partial u}{\partial t} + u\frac{\partial u}{\partial x} + v\frac{\partial u}{\partial y} = 0 \tag{31}$$

$$\frac{\partial v}{\partial t} + u\frac{\partial v}{\partial x} + v\frac{\partial v}{\partial y} = 0 \tag{32}$$

A disturbance is given at a point of the computational domain. Then, its influence on the neighboring points is scrutinized. The above equations are integrated in time both by the present decoupling method and by the explicit second-order Adams–Bashforth method. If a small discrete perturbation $u_c = 1 + \varepsilon$ ($\varepsilon = 0.1$) is given with the initial condition ($u = 1.0$ and $v = 1.0$), the responses to the small perturbation are illustrated in Figure 2 for two CFL numbers, i.e. CFL = 0.2 and 2.0. It is seen that the error distributions computed by the two methods are stable for CFL = 0.2. For a small time step (CFL = 0.2), the response of the initial small perturbation is diminished. However, for a larger time step (CFL = 2.0), the result by the present method is stable as in the case of CFL = 0.2 while the solution of the explicit Adams–Bashforth method is unstable (see Figure 2(c) and (d)). This exemplifies that the present method is stable in the decoupling of velocity components from the implicit convective term.

The validation of the present method is extended to the unsteady laminar cavity flow where the lid moves with a uniform velocity impulsively. The flow in a driven cavity has been used

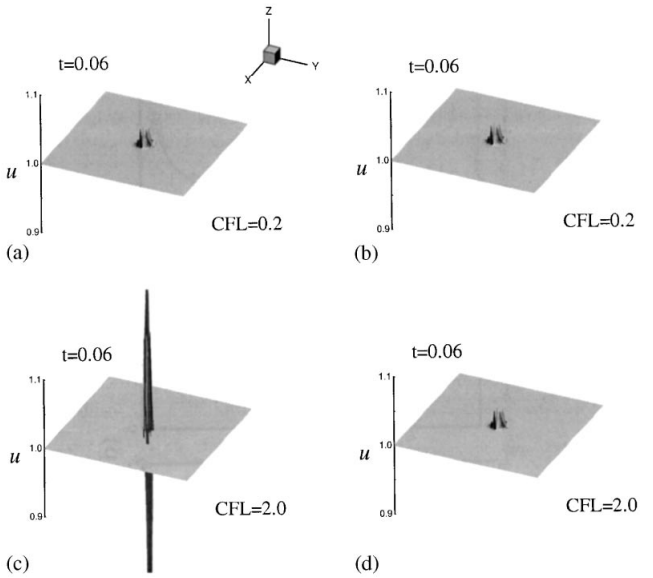

Figure 2. Effects of small discrete perturbation. (a) Adams–Bashforth, CFL = 0.2; (b) present, CFL = 0.2; (c) Adams–Bashforth, CFL = 2.0; (d) present, CFL = 2.0.

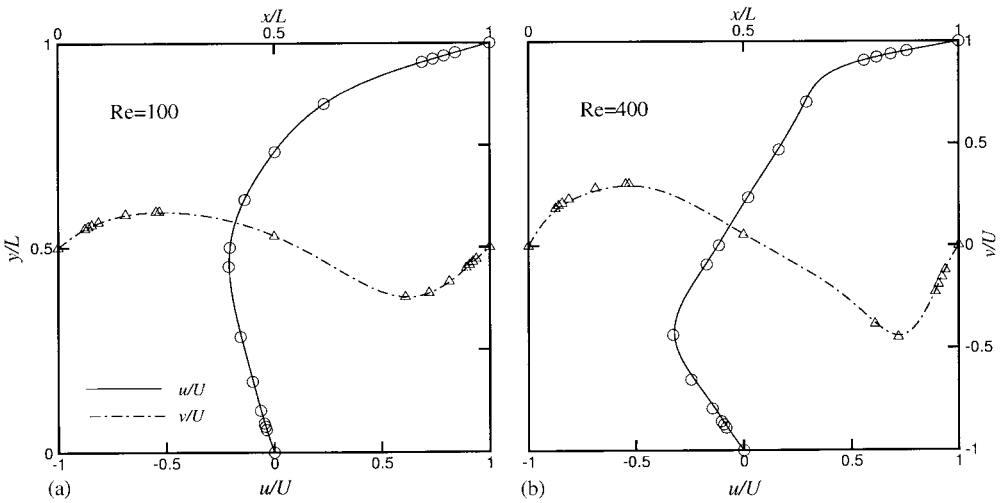

Figure 3. Steady-state centerline velocities. (a) $Re = 100$; (b) $Re = 400$. Symbols from Ghia *et al.* Reference [16].

widely as a standard test case for evaluating the stability and accuracy of numerical methods. Two cases of $Re = 100$ and 400 are solved, where the Reynolds number is defined based upon the side length L and lid velocity U_0. The velocity of the impulsively started lid is given by a step function $u_{\text{lid}} = U_0$ for $t \geqslant 0$ and $u_{\text{lid}} = 0$ for $t < 0$. A 40×40 uniform grid is

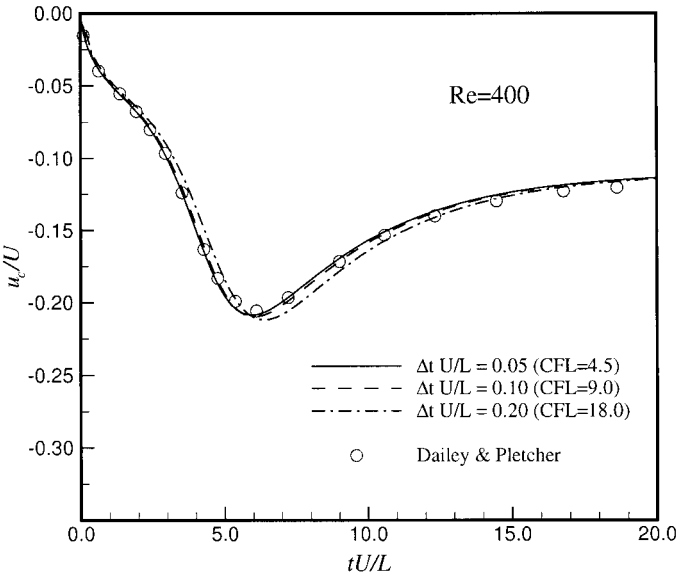

Figure 4. Time history of u at the center for various computational time steps.

used for $Re = 100$ and a 96×96 uniform grid is used for $Re = 400$, respectively. The steady-state centerline velocities are shown for each Reynolds number in Figure 3. As seen, excellent agreement is exhibited with the result of Ghia *et al.* [16]. The time history of u at the center is displayed in Figure 4 and compared with the result of Dailey and Pletcher [17]. The numerical solutions for various computational time steps ($\Delta tU/L = 0.05, 0.10$ and 0.20) are computed for $Re = 400$. These computational time steps correspond to CFL $= 4.5, 9$ and 18, respectively. It is seen that the time history for $\Delta tU/L = 0.10$ is nearly identical with that for $\Delta tU/L = 0.05$. Note that $\Delta tU/L = 0.10$ corresponds to CFL $= 9$. This suggests that the present fully implicit method overcomes the CFL restriction with a trade-off of higher operation counts per time step.

Now, the present fully implicit decoupling method is applied to a direct numerical simulation of turbulent plane channel flow. The Reynolds number is 4200 based on the laminar centerline velocity U_l and the channel half-width δ, which corresponds to $Re_\tau \approx 180$ based on the turbulent wall shear velocity. For the present Reynolds number considered here, the computational domain is chosen to be the minimal channel flow unit of Jiménez and Moin [18]. The streamwise and spanwise computational periods are $\pi\delta$ and $0.289\pi\delta$, respectively (roughly 570 and 160 wall units). The grid points used are $16 \times 129 \times 32$ in the x, y and z directions, respectively. A non-uniform mesh of 129 points with a hyperbolic tangent distribution is used in the wall-normal direction and uniform meshes with spacing $\Delta x^+ \approx 35$ and $\Delta z^+ \approx 5$ are used in the streamwise and spanwise directions, respectively. The first mesh point away from the wall is at $y^+ \approx 0.18$ and the maximum spacing at the centerline of the channel is 7.2 wall units. Since the present computational grid is uniform in the streamwise and spanwise directions with periodic boundary conditions, the three-dimensional Poisson equation in Equation (13) can be reduced to a set of uncoupled one-dimensional equations

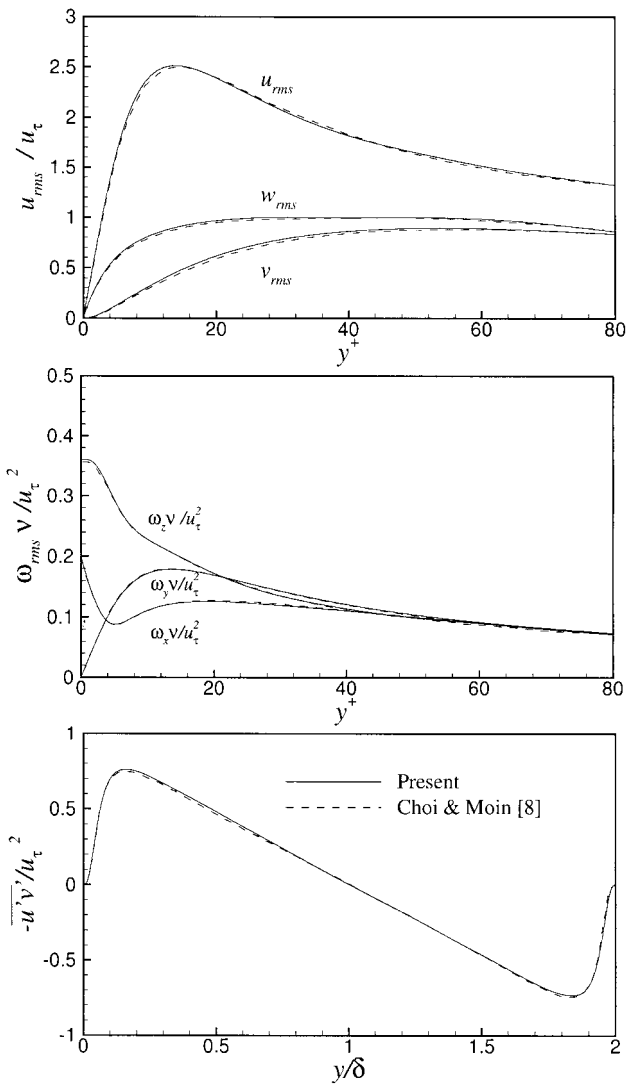

Figure 5. Comparison of the predicted turbulence statistics with those of Choi and Moin [10].

by the two-dimensional Fourier transformation. This requires only the inversion of tridiagonal matrix in the wall-normal direction.

Starting from the laminar velocity profile with random noise, the governing equations are integrated with the computational time step $\Delta t U_l/\delta = 0.02$. The computational time step in the wall unit is $\Delta t^+ = \Delta t u_\tau^2/\nu \approx 0.16$. This is smaller than the time step ($\Delta t^+ \approx 0.4$), which provided an accurate prediction of turbulence statistics in wall-bounded flow [10]. The flow is allowed to develop in time until a statistically steady state is reached. The equations are integrated further in time to obtain the time average of various statistical quantities ($tU/\delta > 200$).

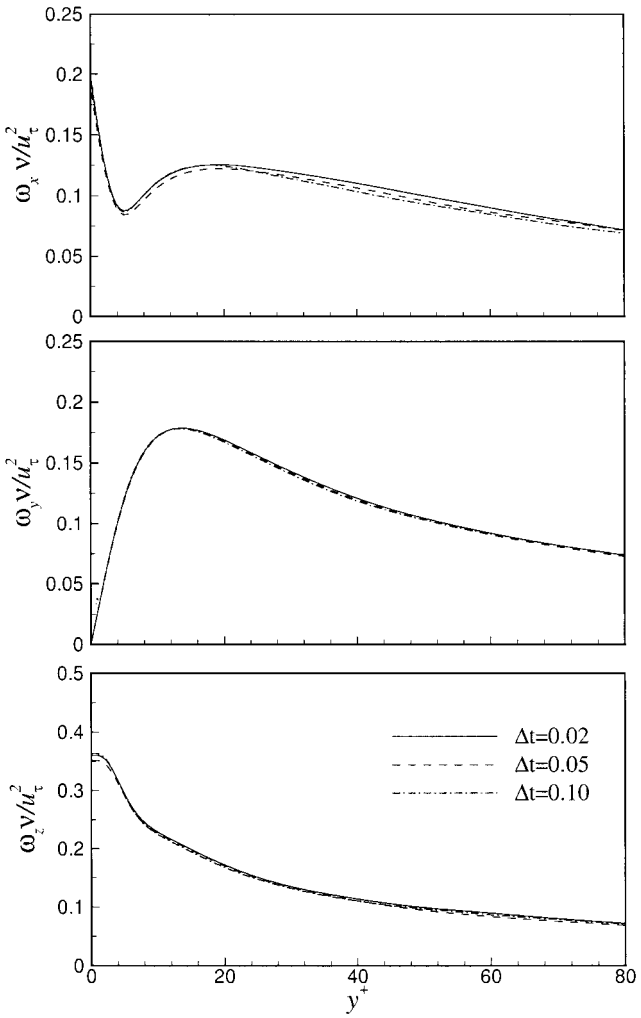

Figure 6. Effect of the computational time step on root-mean-square vorticity fluctuations.

The total averaging time is about $1000\delta/U_l$. The predicted turbulence intensities, root-mean-square vorticity fluctuations normalized by the mean shear at the wall and the Reynolds shear stress profile, are represented in Figure 5. These results are compared with those of Choi and Moin [10], which are obtained by the Newton iterative method for the coupled intermediate velocities. As seen in Figure 5, excellent agreement is shown. This demonstrates that the present fully implicit decoupling method gives an accurate prediction.

The limitation of the computational time step is tested by applying three time steps $\Delta t U_l/\delta = 0.02, 0.05$ and 0.10. These computational time steps correspond to CFL $= 0.4, 1$ and 2, respectively. The initial condition for the instantaneous solution is obtained with $\Delta t U_l/\delta = 0.02$. A closer inspection of the profiles of root-mean-square vorticity fluctuations in Figure 6 discloses that the time step $\Delta t U_l/\delta = 0.10$ is sufficient to predict the turbulence statistics

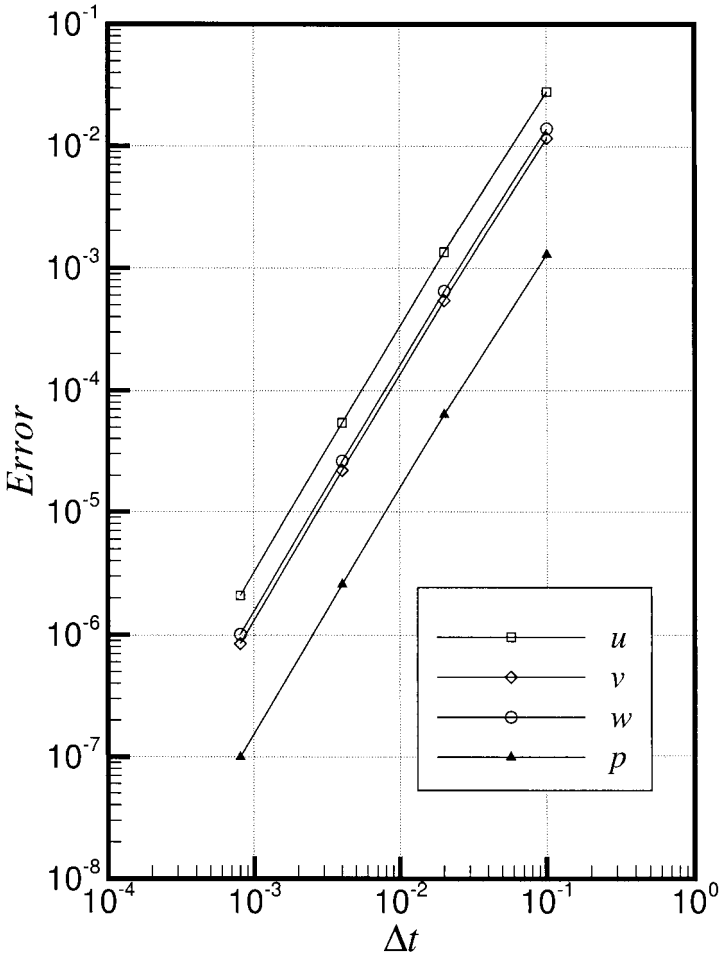

Figure 7. Temporal convergence of the errors.

in wall bounded flow well. Note that $\Delta t U_l/\delta = 0.10$ corresponds to $\Delta t^+ \approx 0.8$ which is larger than $\Delta t^+ \approx 0.4$ of Choi and Moin [10].

Finally, the preservation of the second-order accuracy in time for velocity and pressure is tested in the present turbulent channel flow simulation, where the convection term is significant. The test procedure is the same as that used for Figure 1. As shown in Figure 7, three components of velocity (u, v, w) and pressure (p) maintain the second-order accuracy in time.

4. CONCLUSION

A fully implicit decoupling method for the unsteady incompressible Navier–Stokes equations with second-order accuracy in time has been devised. By straightforward spatial and temporal discretizations, the governing equations were written in a matrix form with the linearized

convection operator. With preserving the second-order accuracy in time, decoupling of the velocity and pressure was made by the block LU decomposition in conjunction with the approximate factorization of the coefficient matrix. In addition, decoupling of the intermediate velocity components was accomplished by the approximate factorization. The temporal second-order accuracy of the present decoupling method has been ascertained by computing the minimal channel flow as well as the two-dimensional vortex flow. The stability of the 'velocity components decoupling' procedure in the present method was checked by the discrete perturbation stability analysis. Simulations of the flow driven by a impulsively started lid in a square cavity confirmed that the present method allows a large time step with the fully implicit time advancement. The present method was applied to the turbulent plane channel flow for several computational time steps. Up to the physical time step of wall bounded turbulent flow, the predicted turbulence statistics were in excellent agreement with those of Choi and Moin [10].

ACKNOWLEDGEMENTS

This research was supported by a grant from the National Research Laboratory of the Ministry of Science and Technology, Korea.

REFERENCES

1. Chorin AJ. Numerical solution of the Navier–Stokes equations. *Mathematics of Computation* 1968; **22**:745–762.
2. Kim J, Moin P. Application of a fractional step method to incompressible Navier–Stokes equations. *Journal of Computational Physics* 1985; **59**:308–323.
3. Bell JB, Colella P, Glaz HM. A second-order projection method for the incompressible Navier–Stokes equations. *Journal of Computational Physics* 1989; **85**:257–283.
4. Van Kan J. A second-order accurate pressure correction scheme for viscous incompressible flow. *SIAM Journal on Scientific and Statistical Computing* 1986; **7**:870–891.
5. Le H, Moin P. An improvement of fractional step methods for the incompressible Navier–Stokes equations. *Journal of Computational Physics* 1991; **92**:369–379.
6. Turek S. Efficient solvers for incompressible flow problems, an algorithmic and computational approach. *Lecture Notes in Computational Science and Engineering*, vol. 6. Springer, 1999.
7. Perot JB. An analysis of the fractional step method. *Journal of Computational Physics* 1993; **108**:51–58.
8. Perot JB. Letter to editor. *Journal of Computational Physics* 1995; **121**:190–191.
9. Dukowicz JK, Dvinsky AS. Approximate factorization as a high order splitting for the implicit incompressible flow equations. *Journal of Computational Physics* 1992; **102**:336–347.
10. Choi H, Moin P. Effects of the computational time step on the numerical solutions of the turbulent flow. *Journal of Computational Physics* 1994; **114**:1–4.
11. Hahn S, Choi H. Unsteady simulation of jets in a cross flow. *Journal of Computational Physics* 1997; **134**:342–356.
12. Rosenfeld M. Uncoupled temporally second-order implicit solver of incompressible Navier–Stokes equations. *AIAA Journal* 1996; **34**:1829–1834.
13. Beam RM, Warming RF. An implicit factored scheme for the compressible Navier–Stokes equations. *AIAA Journal* 1978; **16**:393–402.
14. Akselvoll K, Moin P. Large eddy simulation of turbulent confined coannular jets and turbulent flow over a backward facing step. Report No. TF-63, 1995; Thermosciences Division, Dept of Mechanical Eng, Stanford University.
15. Beam RM, Warming RF. An implicit finite-difference algorithm for hyperbolic systems in conservation law form. *Journal of Computational Physics* 1976; **22**:87–110.
16. Ghia U, Ghia KN, Shin CT. High-*Re* solutions for the incompressible flow using the Navier–Stokes equations and a multigrid method. *Journal of Computational Physics* 1982; **48**:387–411.
17. Dailey LD, Pletcher RH. Evaluation of multigrid acceleration for preconditioned time-accurate Navier–Stokes algorithms. *Computers and Fluids* 1996; **25**:791–811.
18. Jiménez J, Moin P. The minimal flow unit in near-wall turbulence. *Journal of Fluid Mechanics* 1991; **225**:213–240.

